# Design of a High-Foot High-Adiabat ICF Capsule for the National Ignition Facility

T. R. Dittrich,[*] O. A. Hurricane,[†] D. A. Callahan, E. L. Dewald, T. Döppner, D. E. Hinkel, L. F. Berzak Hopkins, S. Le Pape,
T. Ma, J. L. Milovich, J. C. Moreno, P. K. Patel, H.-S. Park, B. A. Remington, and J. D. Salmonson

*Lawrence Livermore National Laboratory, P.O. Box 808, Livermore, California 94551, USA*

J. L. Kline

*Los Alamos National Laboratory, Los Alamos, New Mexico 87545, USA*

(Received 18 September 2013; published 5 February 2014)

The National Ignition Campaign's [M. J. Edwards *et al.*, Phys. Plasmas **20,** 070501 (2013)] point design implosion has achieved DT neutron yields of $7.5 \times 10^{14}$ neutrons, inferred stagnation pressures of 103 Gbar, and inferred areal densities ($\rho R$) of 0.90 g/cm² (shot N111215), values that are lower than 1D expectations by factors of 10×, 3.3×, and 1.5×, respectively. In this Letter, we present the design basis for an inertial confinement fusion capsule using an alternate indirect-drive pulse shape that is less sensitive to issues that may be responsible for this lower than expected performance. This new implosion features a higher radiation temperature in the "foot" of the pulse, three-shock pulse shape resulting in an implosion that has less sensitivity to the predicted ionization state of carbon, modestly lower convergence ratio, and significantly lower ablation Rayleigh-Taylor instability growth than that of the NIC point design capsule. The trade-off with this new design is a higher fuel adiabat that limits both fuel compression and theoretical capsule yield. The purpose of designing this capsule is to recover a more ideal one-dimensional implosion that is in closer agreement to simulation predictions. Early experimental results support our assertions since as of this Letter, a high-foot implosion has obtained a record DT yield of $2.4 \times 10^{15}$ neutrons (within ~70% of 1D simulation) with fuel $\rho R = 0.84$ g/cm² and an estimated ~1/3 of the yield coming from $\alpha$-particle self-heating.

The National Ignition Campaign's (NIC) [1] point design has focused upon keeping the DT fuel adiabat as low as possible, with a four-shock, indirect-drive implosion, to obtain the maximum amount of convergence, thereby reducing the energy required for ignition [2,3]. Achieving this state requires very precise control over hohlraum issues such as drive-related asymmetries and the desired time dependent ablation pressure as well as capsule issues such as managing hydrodynamic instability and mix, delivering the required hot spot formation (set by thermal conductivity of implosion kinetic energy), and attaining sufficient hot spot stagnation pressure (strongly affected by implosion speed) [4,5].

Presently, two-dimensional integrated design simulations (capsule + hohlraum) can only approximately predict the capsule ablation pressure history which can reach a peak of ~100 Mbar over a period of ~10–20 ns. NIF experiments [1,6] indicate that the ablation pressure of the NIC implosion is currently over predicted by ~1.5× during the second pulse, the fourth rise acts as if delayed and reduced, and the peak radiation drive is over predicted by ~15% in flux. This flux deficit in the peak of the drive may be the result of inconsistencies between simulated and actual inner-laser-beam hohlraum penetration and laser entrance hole closure [3,7].

High-mode mix and inadequate hot spot formation likely contribute to less-than-ideal performance of the NIC point design implosion. Implosion velocities > 370 km/s are necessary to create the fuel densification ($\rho R > 1$ g/cm²) and stagnation pressure (> ~400 Gbar) required for high yield but can lead to hydrodynamic instabilities [8–10]. In the few NIC shots where the implosion speed was pushed up above ~300 km/s, and which had less than 8% ablator mass remaining, hot spot ion temperature and yield both dropped significantly and x-ray brightness increased, consistent with ablator material mixing into the center of the implosion [11,12].

Simulations in 2D have not been able to assess correctly the observed mix [2,11] perhaps by overestimating the smoothing effects of ablation-front stabilization or by insufficiently representing the structure on and in the ablator and ice (coming from manufacture or from physics such as species separation effects [13]). Simulations may also underestimate the mass ablated at a given velocity, leading to perhaps more instability feed through from the ablation front [9]. Of course, the 2D simulations do not include 3D effects such as isolated defects in the ablator and/or ice and fill-tube perturbations.

Evidence from nuclear spectra from multiple lines of sight in NIC implosions suggests significant $\rho R$ asymmetry in the assembled cold fuel (with the $\rho R$ at the pole of the capsule measured to be ~2× that of the waist) [5]. This can reduce the efficiency with which implosion kinetic energy
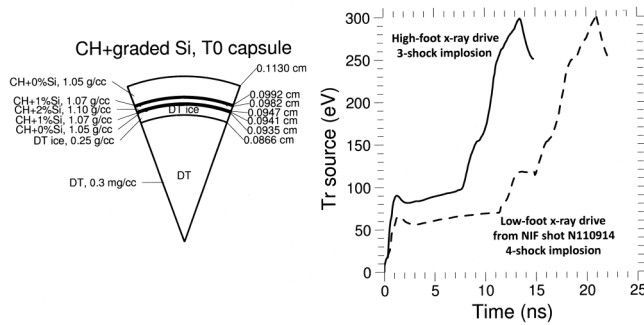
FIG. 1.   The T0 capsule (left) used in the high-foot implosions described here is identical to that used in the majority of the NIC implosions. The radiation temperature (right) driving the high-foot capsule (solid curve), however, is significantly different from that used by the low-foot NIC campaign (dashed curve).



FIG. 2.   The low-foot implosion shock structure (left) has four drive generated shocks and numerous shock reflection and rarefaction features that are not present in the three shock high-foot implosion design (right).

is converted to stagnation pressure resulting in lower stagnation pressures, densities, and yields. For the inferred in-flight fuel adiabat of the NIC implosion, $\alpha \sim 1.5 \pm 0.1$, the inferred hot spot density is $\sim$2–3$\times$ too low, and the fuel $\rho R$ is low by $\sim$15%. A number of factors could contribute to this including mix, low mode asymmetry (hot spot volume), and associated vortex flows, kinetic effects as well as a significant fifth shock.

Stiffer fuel (higher adiabat) [14] implosions would converge less (one can easily show that the convergence ratio $CR \sim p_{abl}^{1/15} v_{imp}^{3/5}/\alpha^{2/5}$) and likely suffer less from mix since lower CR rapidly decreases an implosion's sensitivity to drive nonuniformities and decreases the ultimate growth of instabilities. Experiments at LLE with directly driven cryogenic implosions [15] support the assertion that high adiabat implosions perform closer to 1D model expectations. This assertion may be weakened, however, if increased fuel adiabat is achieved by shock mistiming. Of course, since the energy required for ignition scales as $CR^{-6}$ [16], one cannot completely relax the need to obtain high CR's with facility scale energies of MJs or less.

This Letter gives a description of a three-shock implosion called the high foot—referring to the temperature of the radiation drive in the early part of the drive pulse. The capsule geometry used in this study (see Fig. 1) is identical to the T0 capsule used in the NIC, with a 195 $\mu$m thick ablator [8]. By design, this high-foot implosion is well tuned in that the high adiabat is largely set by the strength of the 1st shock, with the second and third shocks adding a relatively small amount of entropy to the fuel. The pulse shape difference between the high-foot design and a comparison pulse shape taken from a representative implosion fielded by the NIC (shot N110914) is shown in Fig. 1. Characteristic differences are noted in that the high-foot pulse has a higher $T_r$ (90 eV vs 60 eV) and shorter duration (6 ns vs 10 ns) foot and less structure in the main rise to 300 eV radiation temperature, resulting in two additional shocks launched into the ablator rather than three. Figure 2 shows simulated shock plots for a low-foot implosion (left)
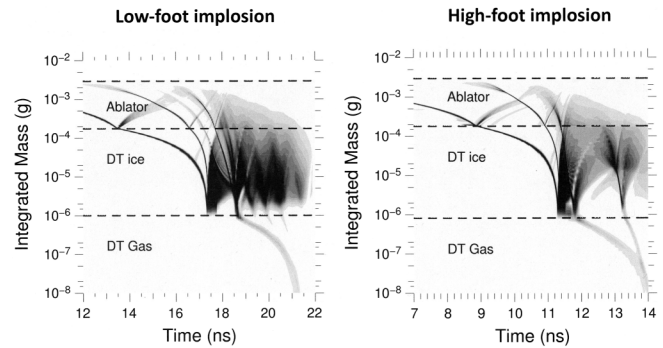
and a high-foot implosion (right). The gray scale shown is proportional to the log derivative of the pressure. Horizontal dashed lines mark interfaces between DT gas, DT ice, and CH ablator. The low-foot implosion exhibits at least four drive-generated shocks, while the high-foot implosion exhibits three drive-generated shocks.

While the higher foot temperature shown in Fig. 1 does in fact raise the fuel adiabat, $\alpha$, the initial motivation for the raised foot temperature was to escape an observed opacity modeling sensitivity in the ablation pressure profile (see Fig. 3). Modeling the low-foot ablation process with a detailed configuration accounting (DCA) opacity model [17] shows disturbing structure in the pressure profile as the second shock propagates through the ablator. This pressure profile structure coincides with the presence of a large amount of carbon in a lithiumlike state (ionization energy of 63 eV). Figure 3 illustrates, in normalized units, the profiles of the charge state distributions (CSD) of carbon, i.e., the fractions of carbon that exist in H-like (black solid), He-like (black dashed), and Li-like (black dotted) states.
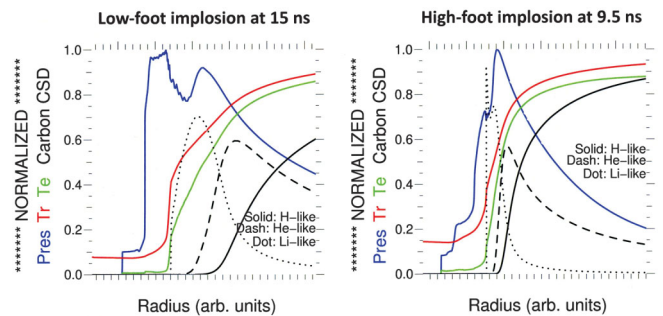


FIG. 3.   For the low-foot implosion (left), DCA modeling of the ablation process shows a distinct double-peak feature in the simulated ablation pressure profile (blue curve) correlated with the location of the carbon Li-like ionization state (black dotted curve). For the high-foot implosion (right), the double-peak feature in the ablation pressure profile is reduced significantly recovering a more ideal profile shape. In each case, the snapshot is taken just before the third drive-generated shock is launched.

TABLE I.  Simulated ideal 1D performance for a low-foot implosion (N110914) and two higher-adiabat, high-foot implosions

|  | 60 eV foot | 80 eV foot | 100 eV foot |
|---|---|---|---|
| $Y$ (MJ) | 16.4 | 3.2 | 0.45 |
| Neutrons | $5.8 \times 10^{18}$ | $1.1 \times 10^{18}$ | $1.6 \times 10^{17}$ |
| $E_{abs}$ (kJ) | 160 | 167 | 168 |
| CR$^a$ at ignition | 36 | 27 | 24 |
| CR$^a$ at bang time$^b$ | 47 | 36 | 40 |
| Fuel $v_{imp}$ (km/s) | 340 | 380 | 390 |
| $P_{stag}$ (GB)$^b$ | 408 | 285 | 294 |
| $\rho R$ fuel (g/cm$^2$) | 1.6 | 1.1 | 1.1 |
| $\Delta S_{fuel}$ (MJ/g/keV) | 454 | 536 | 564 |
| $\alpha$ | 1.45 | 2.28 | 2.8 |
| Normalized $v_{imp}^8/\alpha^4$ | 1$^c$ | 0.4 | 0.16 |

$^a R_{abl}(t=0)/R_{hotspot}$.
$^b \alpha$ deposition off.
$^c$Unity by definition.

The normalized radiation temperature (red curve), electron temperature (green curve), and pressure (blue curve) all show effects of the abundance of Li-like carbon. For the high-foot implosion, the double-peak feature in the ablation pressure profile is reduced significantly as the second shock propagates through the ablator, recovering a more ideal profile shape. Other opacity models, such as super-transition-arrays (STA) [17] do not exhibit such ablation pressure structure. It is anticipated that this structure, if correct, would significantly effect shock timing during capsule implosion. More importantly, this unexpected ablation pressure profile structure could frustrate attempts to retune [1] the implosion.

Various ideal 1D model performance metrics for two different $\alpha$ versions of the high-foot design and the characteristic NIC design are shown in Table I. Ideal 1D performance declines with the high-foot designs, which have lower potential yield ($Y$), stagnation pressure ($P_{stag}$), and $\rho R$. The high-foot designs have higher implosion speed for roughly the same amount of absorbed energy ($E_{abs}$) than the low-foot N110914 (the physics of which is easily understood by recognizing that the high-foot designs ablate more plastic early in time resulting in less ablator mass when the main part of the drive starts). Even with the increased implosion speed, it appears that the 1D margin has been lost in the high-foot designs as measured by the scaling of $v_{imp}^8/\alpha^4$ (a key component of the ignition threshold metric, ITF) [8] while only a modest reduction in CR has been gained. It is not until the 2D stability consequences are examined that the potential benefits and robustness of the high-foot implosion become apparent.

Linear stability analysis of the high-foot implosion has been performed and the growth-factor results (GF, a ratio of initial to final amplitude per mode) are shown in Fig. 4 for the ablation front and fuel-ablator interface. These GFs are sampled at the time of peak implosion velocity. The key
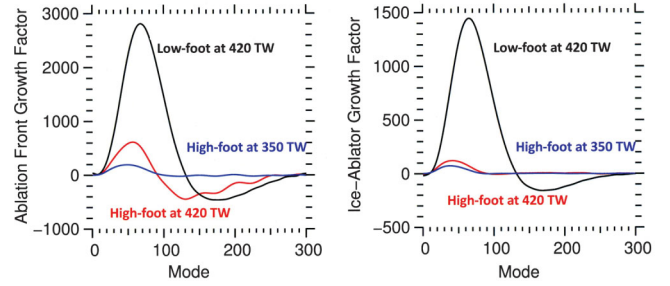


FIG. 4.  The figure compares calculated growth factors (GFs) at the ablation front (left) and ice-ablator interface (right) for the low-foot implosion and high-foot implosion. These GFs are sampled at the time of peak implosion velocity. The primary comparison is between the black curve (low foot at a nominal drive and capsule thickness) and red curve (high foot at nominal drive and capsule thickness) for a 380 km/s implosion and 290 km/s implosion, respectively. The blue curve shows results for a high-foot, low-power implosion as in NIF shot N130501.

comparisons in Fig. 4 are between the red curves (T0 capsule with high-foot pulse shape) and the black curves (T0 capsule with the NIC low-foot nominal power pulse shape). The blue curves represent the GF for the first high-foot DT layered implosion on NIF, shot number N130501 (May 1, 2013).

For the nominal cases of the high-foot pulse versus the low-foot pulse, it is clear that at the ablation front (Fig. 4, left frame) between modes 2–150, the high-foot pulse shows uniformly lower linear instability growth by a factor of about 5. The fuel-ablator interface (Fig. 4, right frame) shows a factor of ~10 less growth for the high foot over the same range of modes from 2–150. The reduced instability growth is rationalized by three primary factors: more
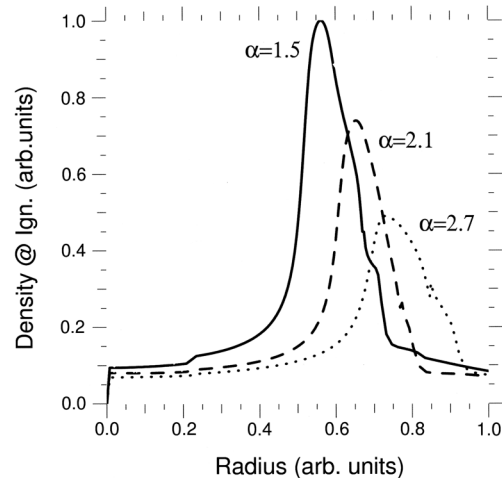


FIG. 5.  Density profiles at ignition time (defined as time when central fuel reaches 12 keV) for various adiabat capsules illustrate reduction in peak ablator density and increase in ablator width as adiabat increases. Values are normalized to the peak value of the $\alpha = 1.5$ curve.
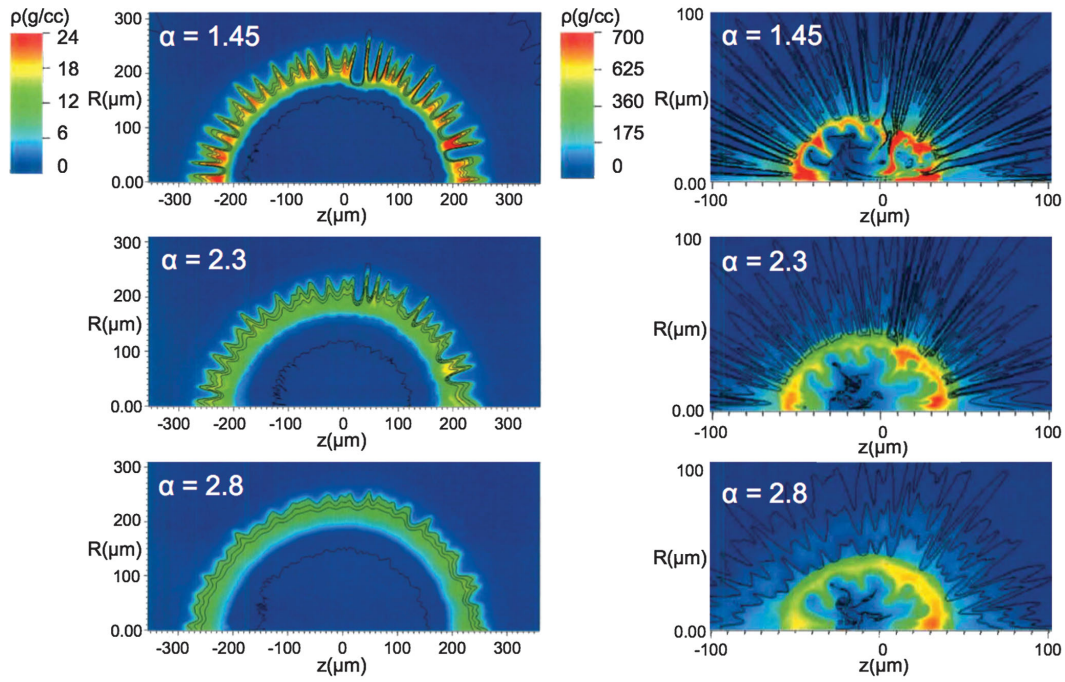
FIG. 6.    Two-dimensional multimode (up to mode 100) simulations with a spectrum of imposed surface roughness (4× nominal) show, in density, the expected instability growth on the capsule. From top to bottom, implosions with $\alpha = 1.45$ (low foot), $\alpha = 2.3$ (high foot), and $\alpha = 2.8$ (high foot) are shown at $R \sim 200$ $\mu m$ (left column) and $R \sim 50$ $\mu m$ (right column).

ablative stabilization due to the higher foot temperature at early times, less Richtmyer-Meshkov instability growth stemming from three rather than four shocks, and a large ablator density gradient scale length (a fluffing out of the ablator) that is sympathetic with the higher adiabat achieved with the higher foot (Fig. 5). Stability gains in the high-foot implosions come at the cost of density compression, for example, at ignition time, the $\alpha = 2.7$ peak density is 50% that of the $\alpha = 1.5$ peak density.

Nonlinear radiation-hydrodynamics simulations up to mode 100 (using the code ARES [18]) confirm the expectation of reduced instability growth (Figs. 6 and 7). These simulations were performed with a multimode specification of the NIC Rev. 5 surface roughness spectrum [8]. Figure 6 shows the results for the $\alpha = 1.5$ N110914 capsule (top two images), the $\alpha = 2.3$ high foot (middle row), and the $\alpha = 2.8$ high foot (bottom row). For clarity, the density color scales in Fig. 6 are fixed for each of the two columns. As $\alpha$ increases, improved stability properties are evident in the reduction in amplitude of correlated RT spikes and bubbles and reduction in high mode number structures at the ablation front and fuel-ablator interface. Figure 7 shows the effect on capsule yield as the initial NIC Rev. 5 surface roughness is arbitrarily increased to a factor of 4× nominal. These hydrodynamic advantages of the high-foot design may be realized if one assumes that the high-foot pulse shape does not substantially degrade the hohlraum or laser-plasma instability (LPI) physics that control the drive on the implosion.

Table II summarizes results from several recent high-foot shots on NIF. The first cryogenic DT high-foot shot, N130501, generated a measured yield within 60% of the 1D simulation. Shot N130710 used significantly higher laser power with a yield 46% of the 1D simulation but had large asymmetries in the observed neutron images. High-foot shot N130812 (August 12th, 2013) returned to
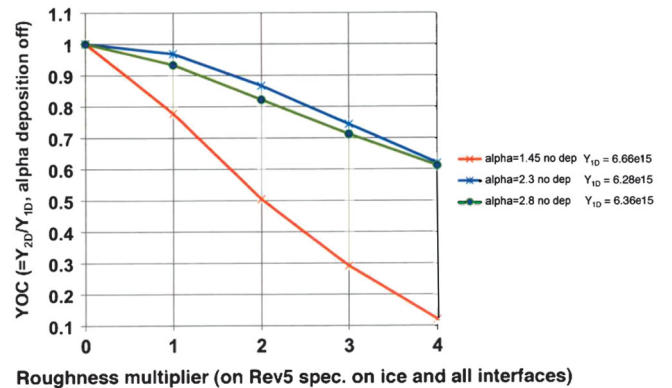


FIG. 7.    Ratios of 2D multimode (up to mode 100) model yields over 1D model yields are plotted vs. a multiplier of the capsule surface roughness for implosions with $\alpha = 1.45$ (low-foot, red), $\alpha = 2.3$ (high-foot, blue), and $\alpha = 2.8$ (high-foot, green) are shown. Even for a roughness multiplier of 4, which drops the simulated 2D yield to 0.1× the 1D yield for the low-foot case, the high-foot implosions only drop to 0.6× the 1D yield consistent with more resistance to ablation front RT instability.

TABLE II.    Performance of three high-foot NIF implosions

|  | N130501 | N130710 | N130812 |
|---|---|---|---|
| Laser power (TW) | 351 | 430 | 355 |
| Laser energy (MJ) | 1.27 | 1.50 | 1.69 |
| Yield (13–15 MeV neutrons) | $0.77 \times 10^{15}$ | $1.0 \times 10^{15}$ | $2.4 \times 10^{15}$ |
| Bang time (ns) | 16.7 | 16.4 | 16.7 |
| $T_{\mathrm{ion}}$ (keV) | 3.0 | 3.5 | 4.2 |
| $\rho R$ fuel (g/cm$^2$) | 0.6 | 0.7 | 0.9 |
| Neutron burn width (ns) | 0.172 | 0.180 | 0.156 |

low laser power but had high laser energy and generated a yield within 70% of the 1D simulation. For N130812, 10.3 kJ of energy (kinetic + internal, both at peak velocity, $+pdV$ work on fuel between the time of peak velocity and peak burn) was delivered to the DT fuel, with 8 kJ of fusion energy produced. About 3 kJ of this fusion energy is estimated to originate in $\alpha$-particle self-heating. This estimate is based on 1D implosion simulations with $\alpha$-heating enabled compared with simulations with $\alpha$-heating disabled. Details of these high-foot DT experiments are presented in a companion paper by Park et al. [19].

It is likely that the high-foot inertial confinement fusion capsule described here is not an end onto itself. This capsule implosion was designed to be insensitive to 2D and 3D hydrodynamic defects and demonstrate performance close to 1D expectations; this prediction has been verified by recent experiments. However, according to simulations, the ultimate performance of this simplified implosion is limited. The superior results obtained from these high-foot experiments allow several aspects of the integrated ignition platform to be examined and understood. Future variations in capsule design (such as thinning the ablator) and hohlraum parameters (such as increasing the peak laser power) from that presented here may be able to increase implosion velocity and lead to further improvements. Making these variations in small incremental steps from the demonstrated performance points of the high-foot capsule described here will help identify and perhaps

improve the limits of predictive capabilities of models used in the design process.

*dittrich1@llnl.gov
†hurricane1@llnl.gov

[1] O. L. Landen et al., Phys. Plasmas **18**, 051002 (2011).
[2] M. J. Edwards et al., Phys. Plasmas **20**, 070501 (2013).
[3] H. F. Robey et al., Phys. Plasmas **20**, 052707 (2013).
[4] D. S. Clark et al., Phys. Plasmas **20**, 056318 (2013).
[5] C. Cerjan, P. T. Springer, and S. M. Sepke, Phys. Plasmas **20**, 056319 (2013).
[6] D. G. Hicks, B. K. Spears, D. G. Braun, R. E. Olson, C. M. Sorce, P. M. Celliers, G. W. Collins, and O. L. Landen, Phys. Plasmas **17**, 102703 (2010).
[7] S. A. Maclaren et al., LLNL Report No. LLNL-PRES-595273.
[8] S. W. Haan et al., Phys. Plasmas **18**, 051001 (2011).
[9] N. B. Meezan et al., Phys. Plasmas **20**, 056311 (2013).
[10] D. G. Hicks et al., Phys. Plasmas **19**, 122702 (2012).
[11] T. Ma et al., Phys. Rev. Lett. **111**, 085004 (2013).
[12] M. A. Barrios et al., Phys. Plasmas **20**, 072706 (2013).
[13] P. Amendt, C. Bellei, and S. Wilks, Phys. Rev. Lett. **109**, 075002 (2012).
[14] V. N. Gonchorov and O. A. Hurricane, LLNL Report No. LLNL-TR-562104, 2012; LLNL Report No. LLNL-TR-570412, 2012.
[15] T. C. Sangster et al., Phys. Plasmas **20**, 056317 (2013).
[16] S. Atzeni and J. Meyer-ter-Vehn, The Physics of Inertial Fusion (Clarendon Press, Oxford, 2004), p. 68.
[17] J. I. Castor, Radiation Hydrodynamics (Cambridge University Press, Cambridge, England, 2004), p. 172.
[18] R. M. Darlington, T. McAbee, and G. Rodrigue, Comput. Phys. Commun. **135**, 58 (2001).
[19] H.-S. Park et al., preceding Letter, Phys. Rev. Lett. **112**, 055001 (2014).